Supporting Information
for
Rethinking the existence of hexagonal sodium zirconate CO_2 sorbent

Ribooga Chang[a], Ashok S. Menon[b], Erik Svensson Grape[c], Peter Broqvist[d], A. Ken Inge[c] and Ocean Cheung[a]

[a] Division of Nanotechnology and Functional Materials, Department of Materials Science and Engineering, Uppsala University, Ångström Laboratory, Uppsala SE-751 03, Box 35, Sweden

[b] WMG, University of Warwick, Coventry CV4 7AL, United Kingdom

[c] Department of Materials and Environmental Chemistry, Stockholm University, SE-10691, Sweden

[d] Division of Structural Chemistry, Department of CHemistry, Uppsala University, Ångström Laboratory, Uppsala SE-751 03, Box 35, Sweden

[*]Corresponding author. Tel.: +46 18 471 3279, Email:ocean.cheung@angstrom.uu.se

Table of Contents

Section 1. Simulated PXRD patterns of sodium zirconate (sodium zirconium oxide; Na_2ZrO_3)

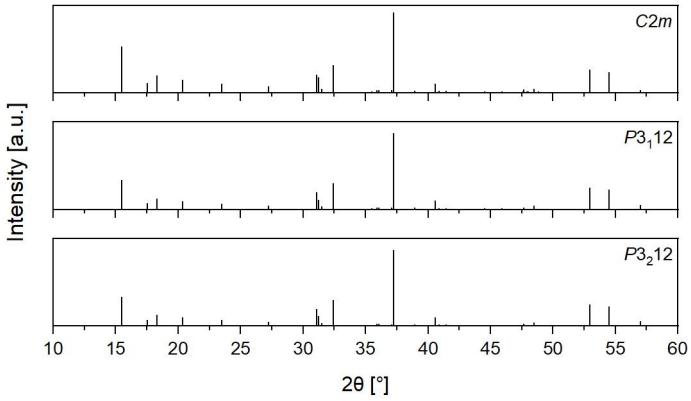

Figure S1. The simulated XRD patterns of the determined three space groups: *C*2/*m*, *P*3$_1$12, and *P*3$_2$12 of sodium zirconium oxide (Na_2ZrO_3).

1.1 DIFFaX simulations for the stacking faults

XRD patterns (Cu-Kα) were simulated over 10 – 80° (2θ) with a step size of 0.02°. A pseudo-Voigt peak shape function was chosen with parameters from the Caglioti equation u = 0.15, v = −0.036, w = 0.009, and a Lorentzian contribution of σ = 0.6, in order to imitate experimental conditions. An infinite number of layers with a recursive stacking sequence was used in the simulation. Stacking fault and Na-Zr ordering degree were varied in the simulations. The Na_2ZrO_3 model was prepared following the transformations detailed in Serrano-Sevillano et al.,[1] where the conventional monoclinic unit cell was transformed into the triclinic system with a P space group. The triclinic model contains an Na layer (L_1) and aa Na-Zr-O layer (L_2). The details of the structure are:

Table S1. Details of the structure model used for X-ray simulations and refinement. B_{iso} denotes the isotropic temperature parameter.

Unit cell parameters						
	a, b (Å)		c (Å)		γ (°)	
	5.6250		5.4850		60.097	
Layer compositions						
Layer	Atom	x/a	y/b	z/c	Occupancy	B_{iso}

L_1	Na	0	0	0	1	1
	Na	1/3	1/3	0	1	1
	Na	2/3	2/3	0	1	1
L_2, L_3 and L_4	Na	0	0	0	1.0	1
	Zr	1/3	1/3	0	1.0	1
	Zr	2/3	2/3	0	1.0	1
	O	0.340	0.000	0.225	1	1
	O	0.650	0.000	−0.225	1	1
	O	0.000	0.340	−0.225	1	1
	O	0.340	0.650	−0.225	1	1
	O	0.650	0.340	0.225	1	1
	O	0.000	0.650	0.225	1	1

Three different stacking vectors were used to generate stacking faults, (1/3, −1/3, 1/2), (2/3, 0, 1/2), and (0, −2/3, 1/2). Each represent different stacking of the Na-Zr-O layer with respect to the Na layer. The three resulting layers, L_2, L_3, and L_4, are compositionally similar but stacked differently compared to L_1. These stacking sequences are described as R (rectangular, L_2), P (parallelogram, L_3), and P′ (parallelogram, L_4).[38] An L_1 - L_2 - L_1 - L_2… stacking corresponds to the ideal crystal structure with no faults. By varying the probability of occurrence of each of the stacking vectors, stacking faults are then generated. Varying degrees of stacking faults were generated in LMO using the methodology defined elsewhere.[2] Using this definition, the degree of faulting or stacking fault probability is defined:

$$\text{Stacking fault probability (\%)} = \frac{1-P_{L2}}{2/3} \times 100$$

Where, PL_2 is the probability of the occurrence (translation probability) of the L_2 layer given by (1/3, −1/3, 1/2) stacking after L_1.

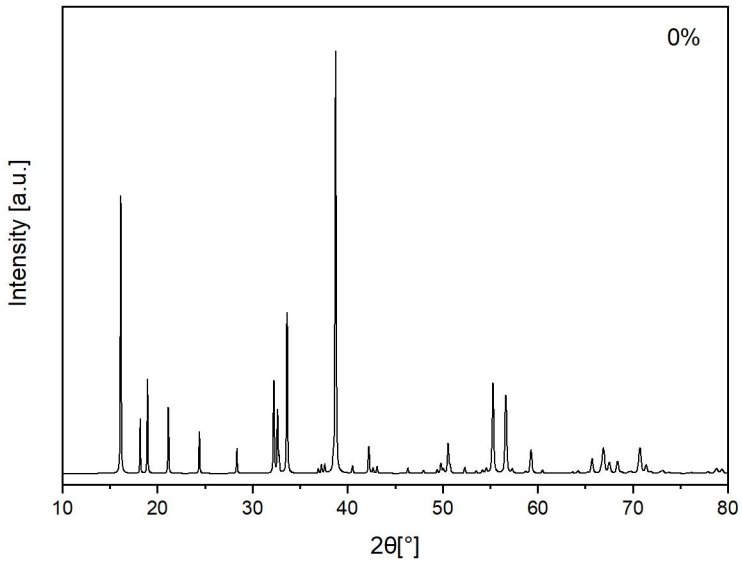

Figure S2. Simulated diffraction pattern of Na_2ZrO_3 with 0 % stacking fault (2θ range = 10 to 80°, λ = 1.54056 Å).

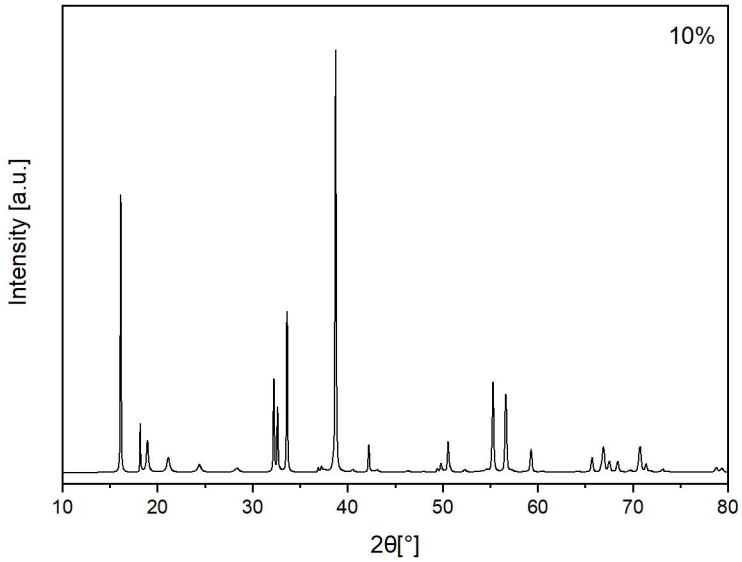

Figure S3. Simulated diffraction pattern of Na_2ZrO_3 with 10 % stacking fault (2θ range = 10 to 80°, λ = 1.54056 Å).

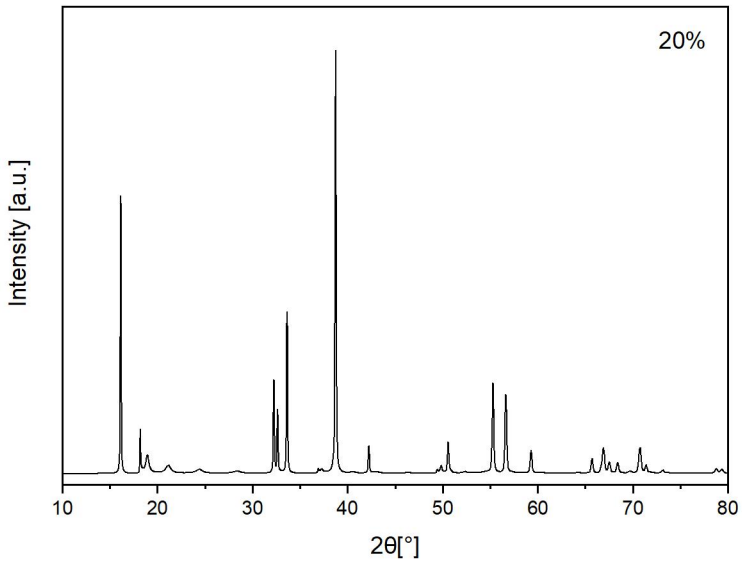

Figure S4. Simulated diffraction pattern of Na_2ZrO_3 with 20 % stacking fault (2θ range = 10 to 80°, λ = 1.54056 Å).

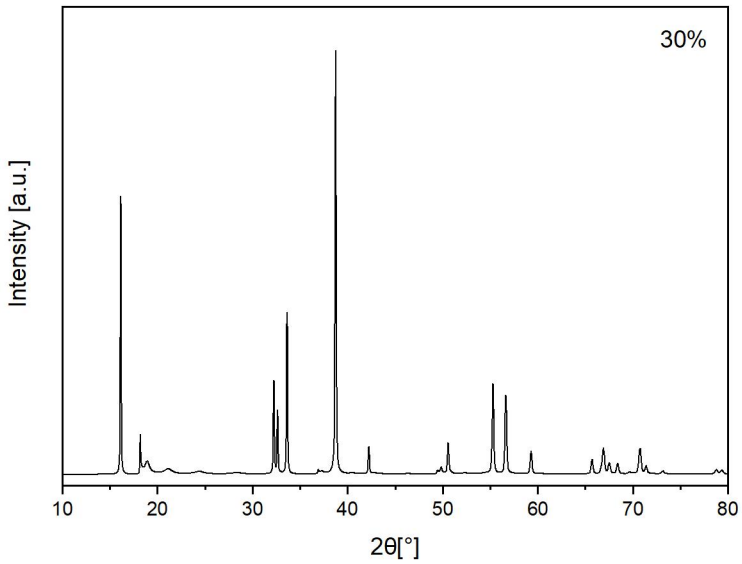

Figure S5. Simulated diffraction pattern of Na_2ZrO_3 with 30 % stacking fault (2θ range = 10 to 80°, λ = 1.54056 Å).

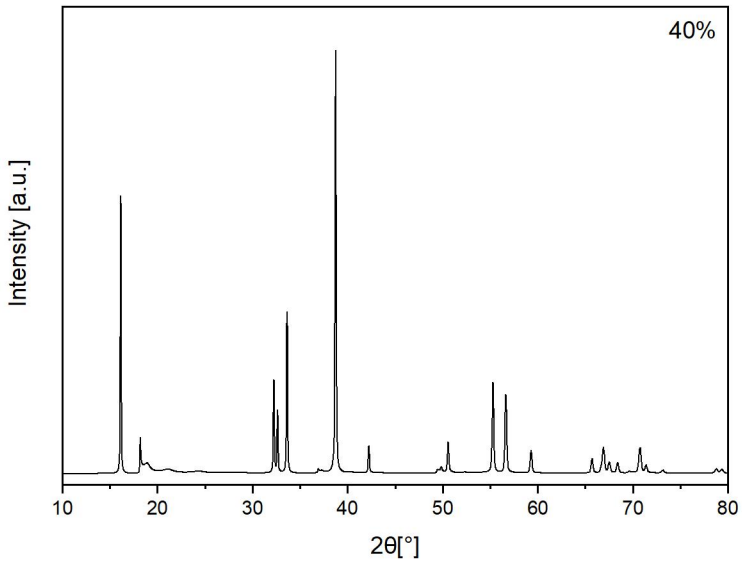

Figure S6. Simulated diffraction pattern of Na_2ZrO_3 with 40 % stacking fault (2θ range = 10 to 80°, λ = 1.54056 Å).

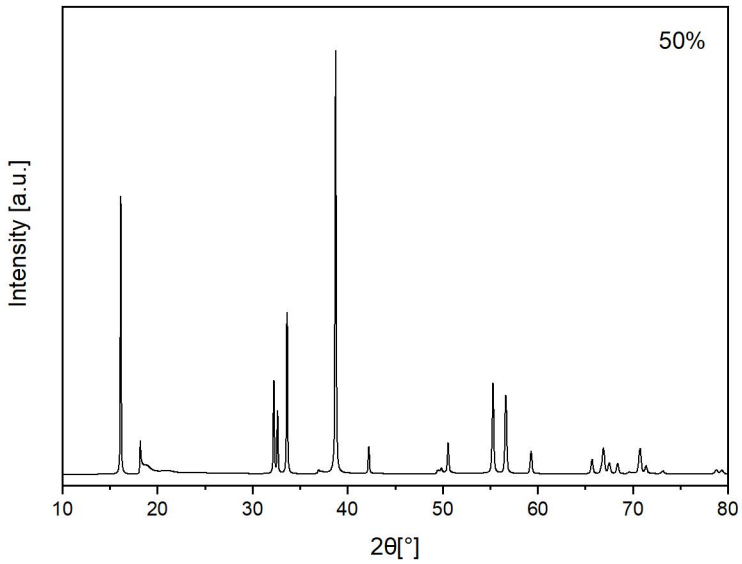

Figure S7. Simulated diffraction pattern of Na_2ZrO_3 with 50 % stacking fault (2θ range = 10 to 80°, λ = 1.54056 Å).

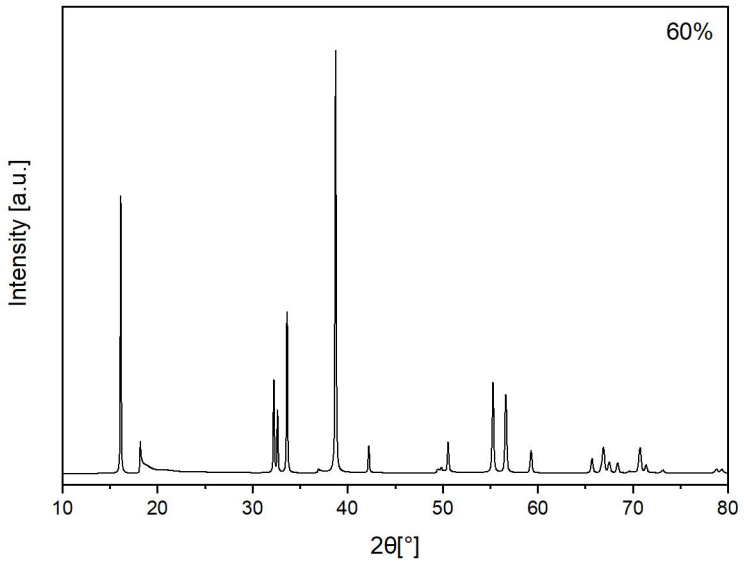

Figure S8. Simulated diffraction pattern of Na_2ZrO_3 with 60 % stacking fault (2θ range = 10 to 80°, λ = 1.54056 Å).

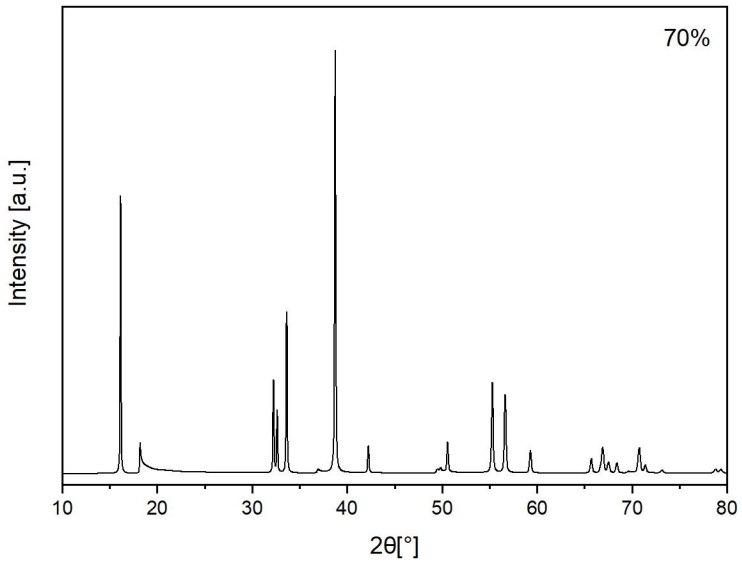

Figure S9. Simulated diffraction pattern of Na_2ZrO_3 with 70 % stacking fault (2θ range = 10 to 80°, λ = 1.54056 Å).

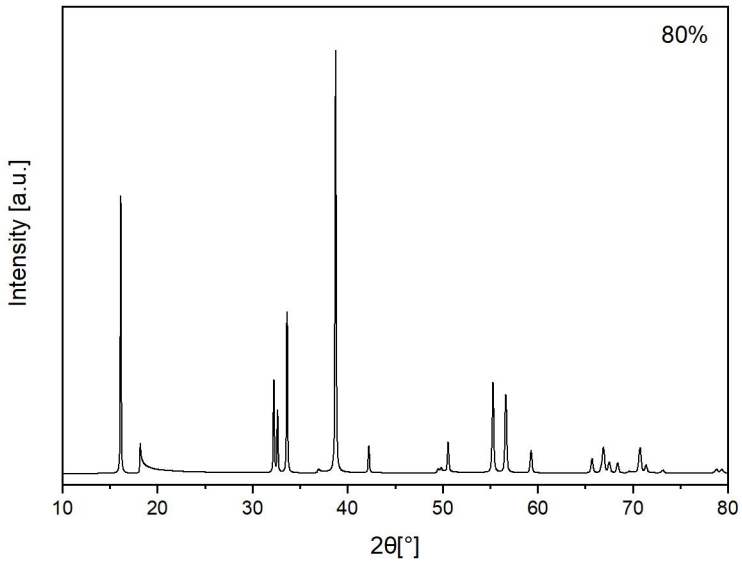

Figure S10. Simulated diffraction pattern of Na_2ZrO_3 with 80 % stacking fault (2θ range = 10 to 80°, λ = 1.54056 Å).

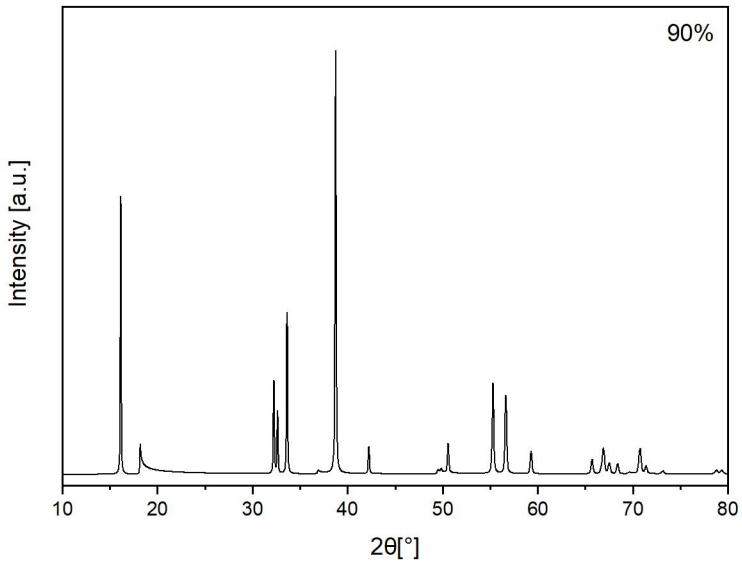

Figure S11. Simulated diffraction pattern of Na_2ZrO_3 with 90 % stacking fault (2θ range = 10 to 80°, λ = 1.54056 Å).

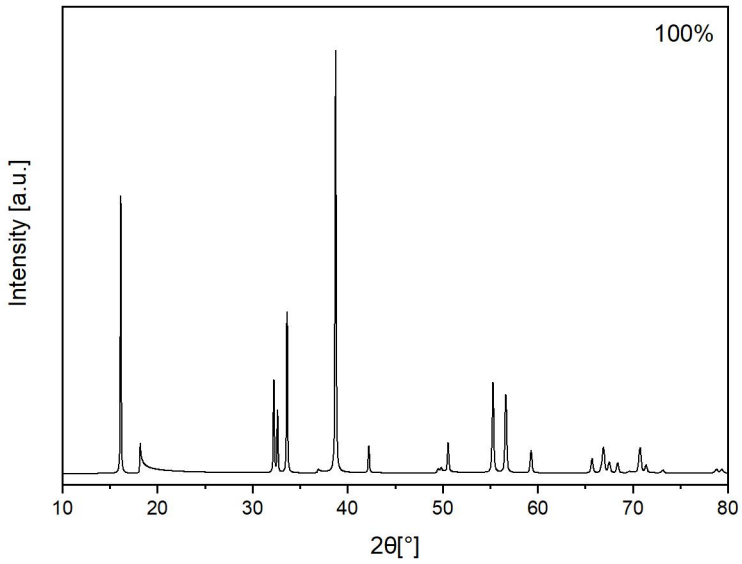

Figure S12. Simulated diffraction pattern of Na_2ZrO_3 with 100 % stacking fault (2θ range = 10 to 80°, λ = 1.54056 Å).

1.2 DIFFaX simulations of cation site mixing

As per the definition of the crystallographic unit cell used for the simulations, different degrees of Na-Zr site mixing were created arbitrarily by varying the site occupancies of the Na and Zr sites in the Na-Zr-O layer. This layer has one Na and two crystallographically distinct Zr sites. For simplicity, the occupancies (occ) of the two Zr sites were fixed to be equal. The different degrees of Na-Zr site mixing and the corresponding occupancy of each site are shown below. The degree of Na-Zr site mixing has been defined in terms of the occupancy of Zr on the Na site, where a value of 50% refers to 50% probability of finding Zr at the Na site.

Table S2. Relationship between the overall Na-Zr site mixing and the occupancies of Na and Zr.

Na-Zr site mixing (%)	Na site (Na occ/Zr occ)	Zr site1 (Na occ/Zr occ)	Zr site2 (Zr occ/Na occ)
$0 \rightarrow 0$	1/0	1/0	1/0
$0.1 \rightarrow 10\%$	0.9/0.1	0.95/0.05	
$0.2 \rightarrow 20\%$	0.8/0.2	0.9/0.1	0.9/0.1
$0.3 \rightarrow 30\%$	0.7/0.3	0.85/0.15	0.85/0.15
$0.4 \rightarrow 40\%$	0.6/0.4	0.8/0.2	0.8/0.2
$0.5 \rightarrow 50\%$	0.5/0.5	0.75/0.25	0.75/0.25

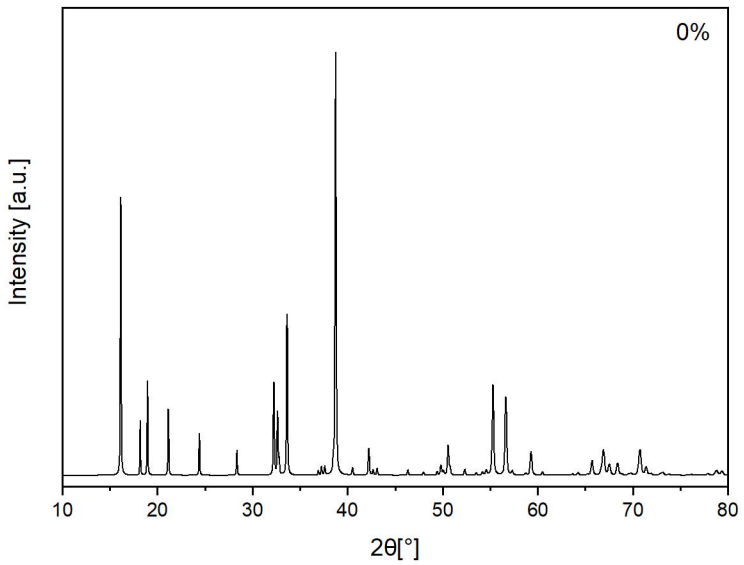

Figure S13. Simulated diffraction pattern of Na_2ZrO_3 with 0 % cation site mixing (2θ range = 10 to 80°, λ = 1.54056 Å).

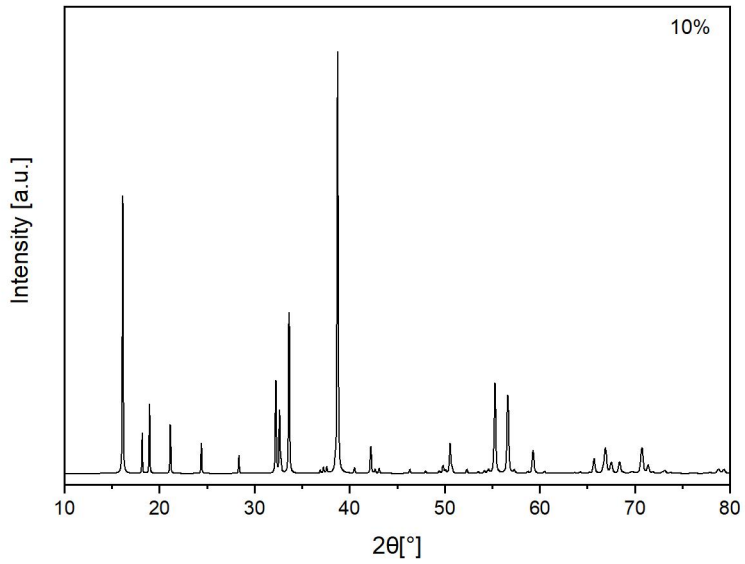

Figure S14. Simulated diffraction pattern of Na_2ZrO_3 with 10 % cation site mixing (2θ range = 10 to 80°, λ = 1.54056 Å).

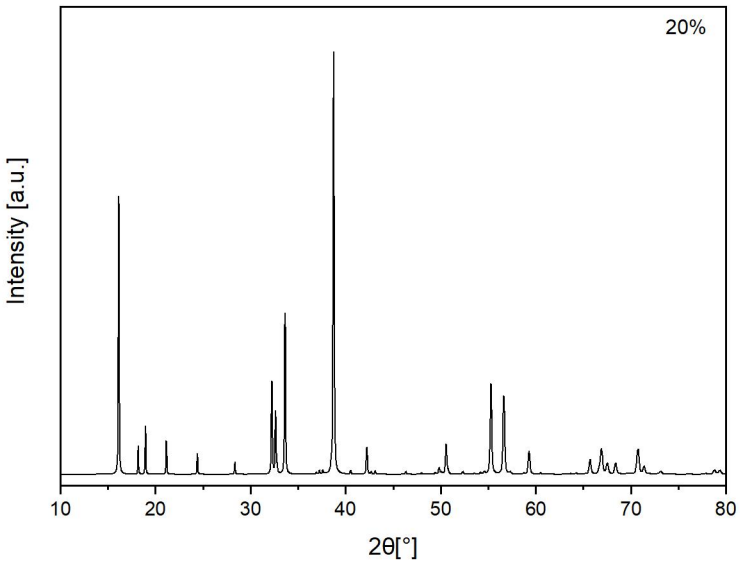

Figure S15. Simulated diffraction pattern of Na_2ZrO_3 with 20 % of the cation site mixing (2θ range = 10 to 80°, λ = 1.54056 Å).

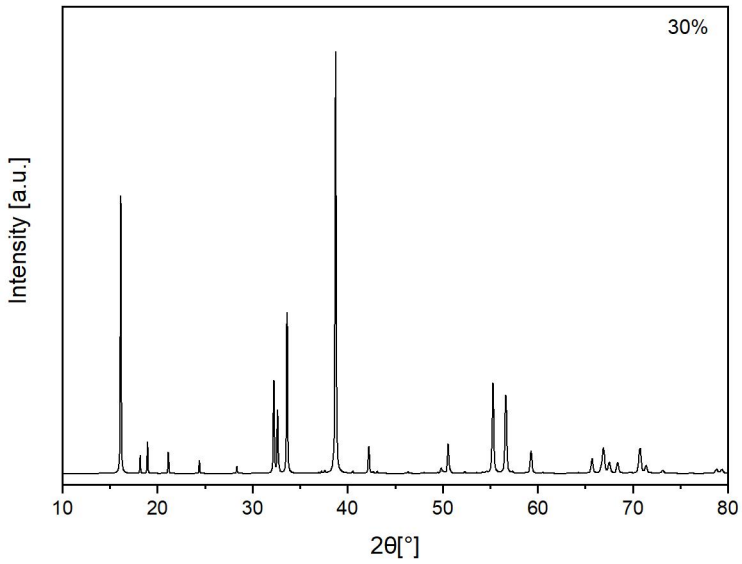

Figure S16.Simulated diffraction pattern of Na_2ZrO_3 with 30 % cation site mixing (2θ range = 10 to 80°, λ = 1.54056 Å).

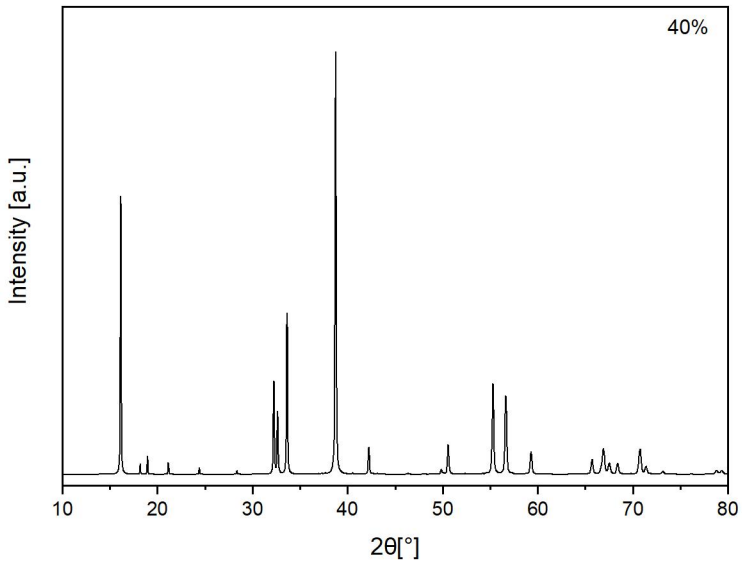

Figure S17. Simulated diffraction pattern of Na_2ZrO_3 with 40 % cation site mixing (2θ range = 10 to 80°, λ = 1.54056 Å).

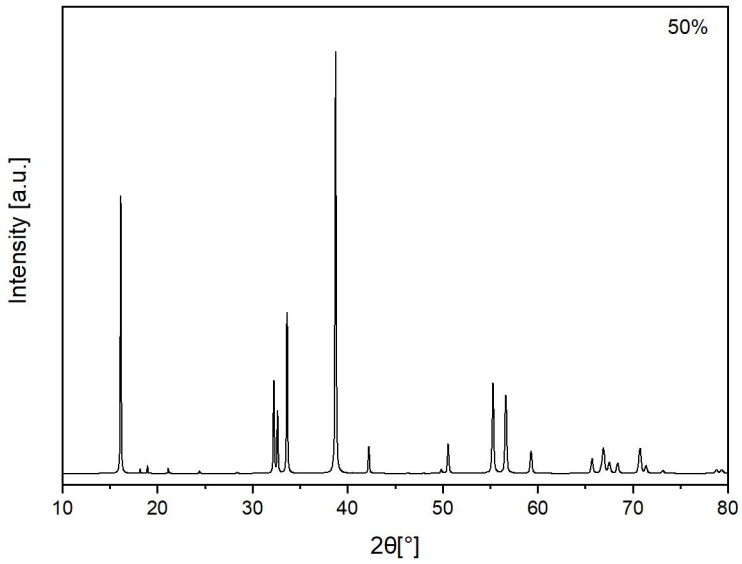

Figure S18. Simulated diffraction pattern of Na_2ZrO_3 with 50 % cation site mixing (2θ range = 10 to 80°, λ = 1.54056 Å).

1.3 Diamond simulations for the Na^+ site occupancy

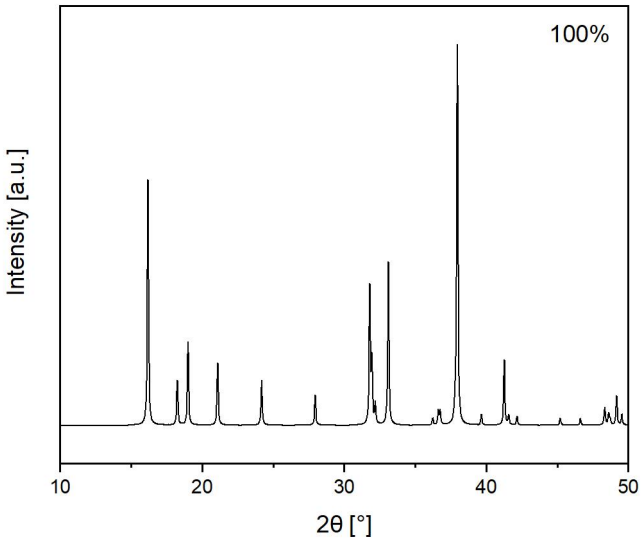

Figure S19. Simulated diffraction pattern of monoclinic Na_2ZrO_3 (*C*2/*m*) with 100 % Na^+ site occupancy of the Na layer (2θ range = 10 to 50°, λ = 1.54056 Å).

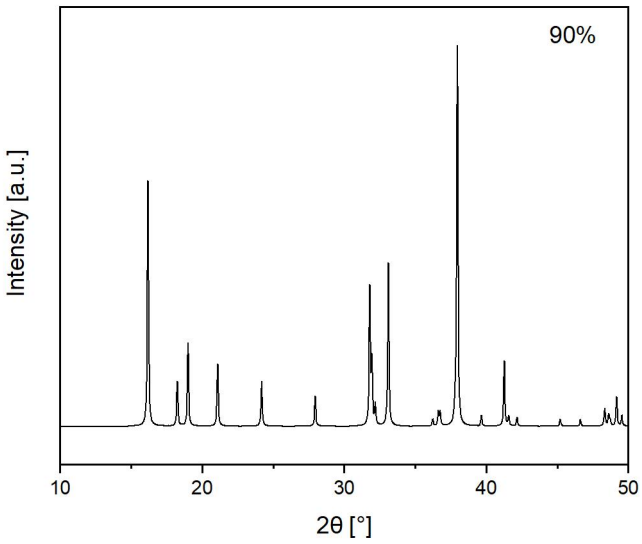

Figure S20. Simulated diffraction pattern of monoclinic Na_2ZrO_3 (*C*2/*m*) with 90 % Na^+ site occupancy of the Na layer (2θ range = 10 to 50°, λ = 1.54056 Å).

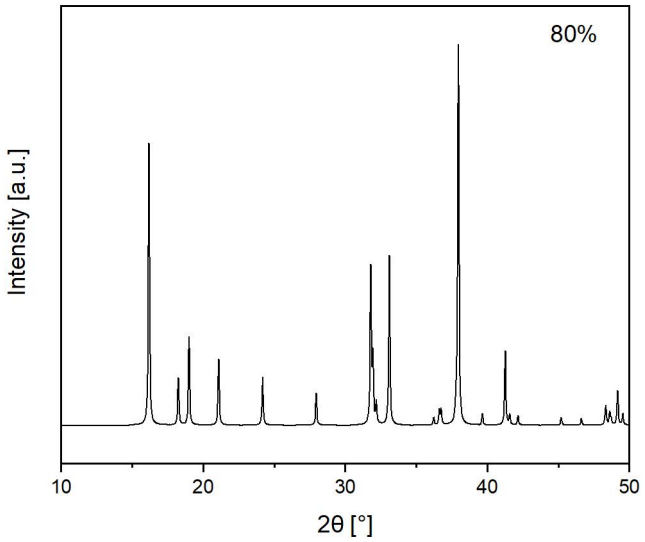

Figure S21. Simulated diffraction pattern of monoclinic Na_2ZrO_3 (*C*2/*m*) with 80 % Na^+ site occupancy of the Na layer (2θ range = 10 to 50°, λ = 1.54056 Å).

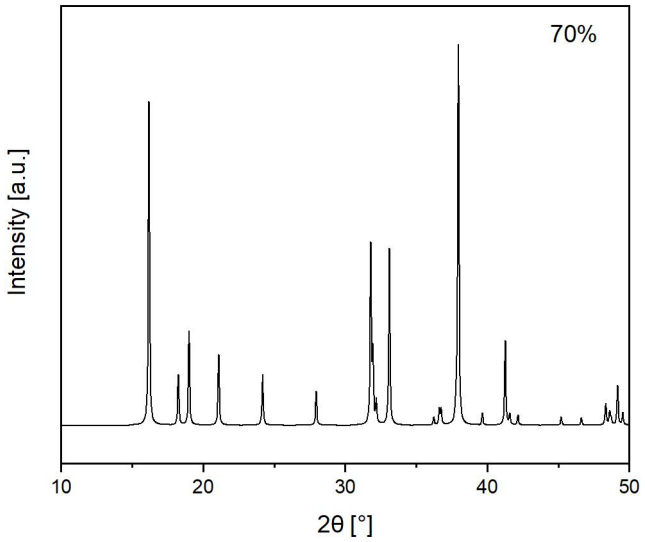

Figure S22. Simulated diffraction pattern of monoclinic Na_2ZrO_3 (*C*2/*m*) with 70 % Na^+ site occupancy of the Na layer (2θ range = 10 to 50°, λ = 1.54056 Å).

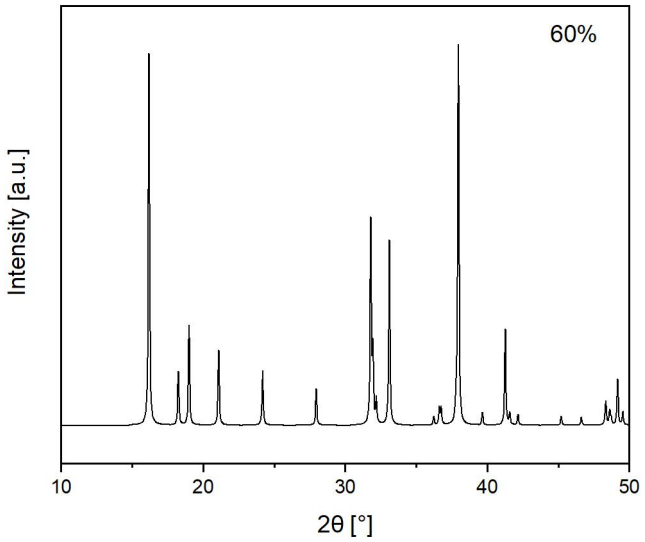

Figure S23. Simulated diffraction pattern of monoclinic Na_2ZrO_3 (*C*2/*m*) with 60 % Na^+ site occupancy of the Na layer (2θ range = 10 to 50°, λ = 1.54056 Å).

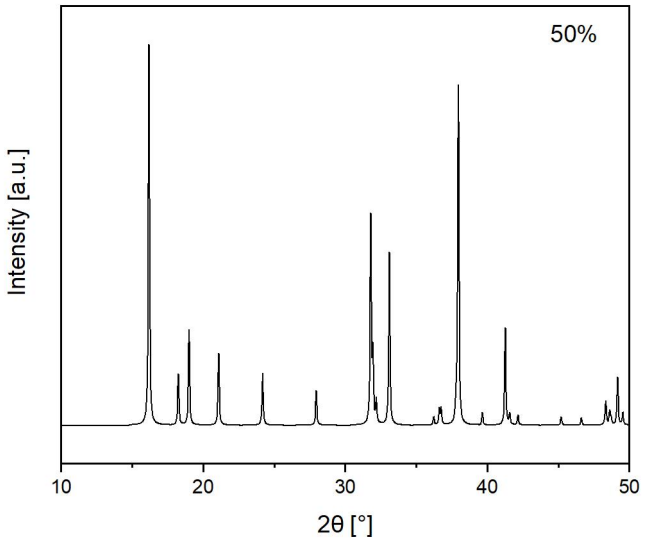

Figure S24. Simulated diffraction pattern of monoclinic Na_2ZrO_3 (*C*2/*m*) with 50 % Na^+ site occupancy of the Na layer (2θ range = 10 to 50°, λ = 1.54056 Å).

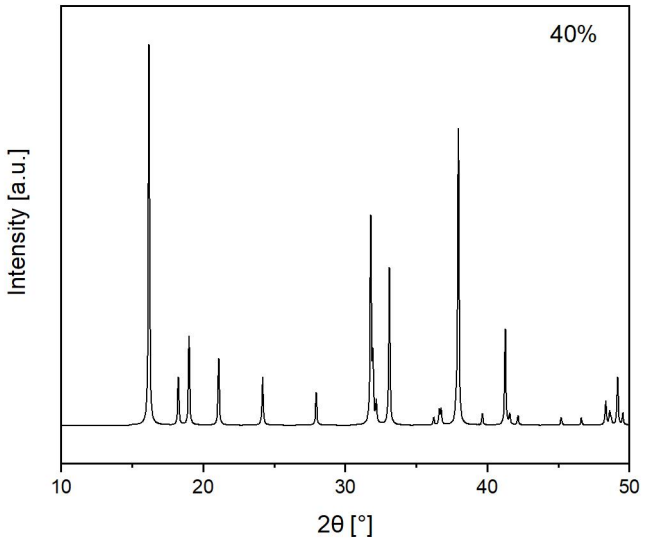

Figure S25. Simulated diffraction pattern of monoclinic Na_2ZrO_3 (*C*2/*m*) with 40 % Na^+ site occupancy of the Na layer (2θ range = 10 to 50°, λ = 1.54056 Å).

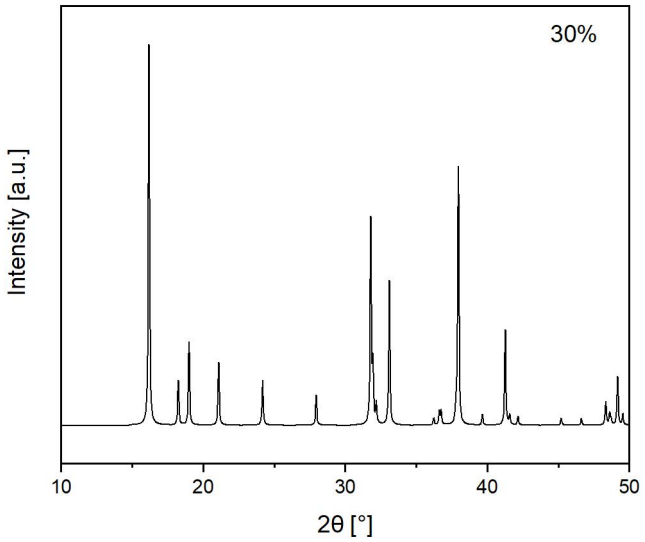

Figure S26. Simulated diffraction pattern of monoclinic Na_2ZrO_3 (*C*2/*m*) with 30 % Na^+ site occupancy of the Na layer (2θ range = 10 to 50°, λ = 1.54056 Å).

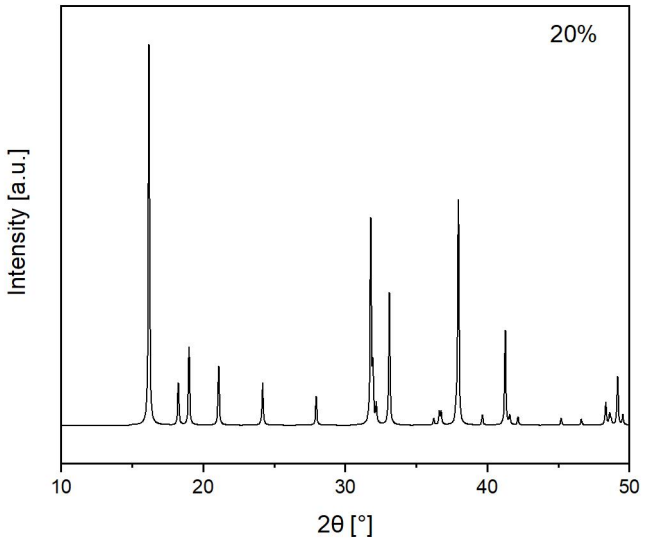

Figure S27. Simulated diffraction pattern of monoclinic Na_2ZrO_3 (*C*2/*m*) with 20 % Na^+ site occupancy of the Na layer (2θ range = 10 to 50°, λ = 1.54056 Å).

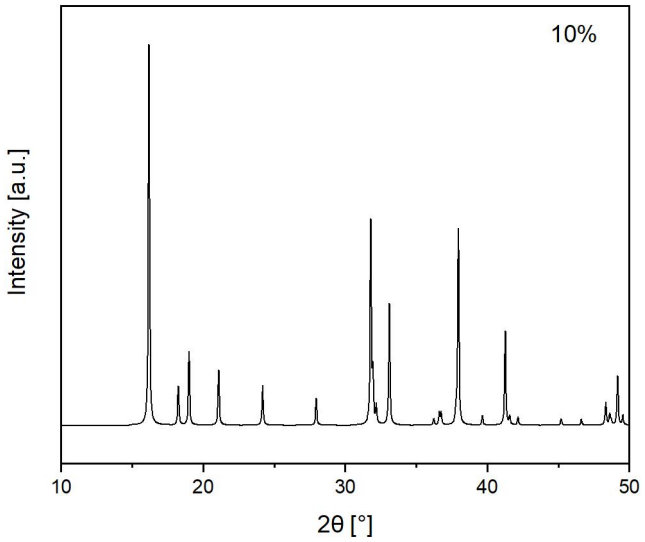

Figure S28. Simulated diffraction pattern of monoclinic Na_2ZrO_3 (*C*2/*m*) with 10 % Na^+ site occupancy of the Na layer (2θ range = 10 to 50°, λ = 1.54056 Å).

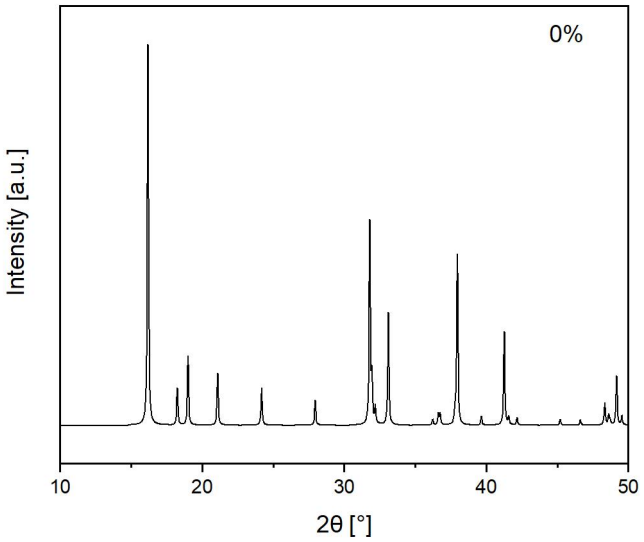

Figure S29. Simulated diffraction pattern of monoclinic Na_2ZrO_3 (*C*2/*m*) with 0 % Na^+ site occupancy of the Na layer (2θ range = 10 to 50°, λ = 1.54056 Å).

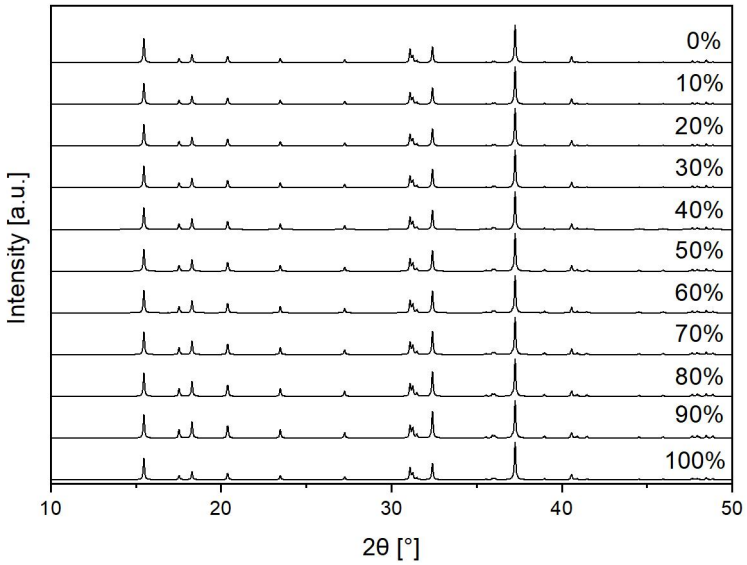

Figure S30. Simulated diffraction pattern of monoclinic Na_2ZrO_3 (*C*2/*m*) with 100 to 0 % Na^+ site occupancy of the $Na^+ + Zr^{4+}$ layer (2θ range = 10 to 50°, λ = 1.54056 Å).

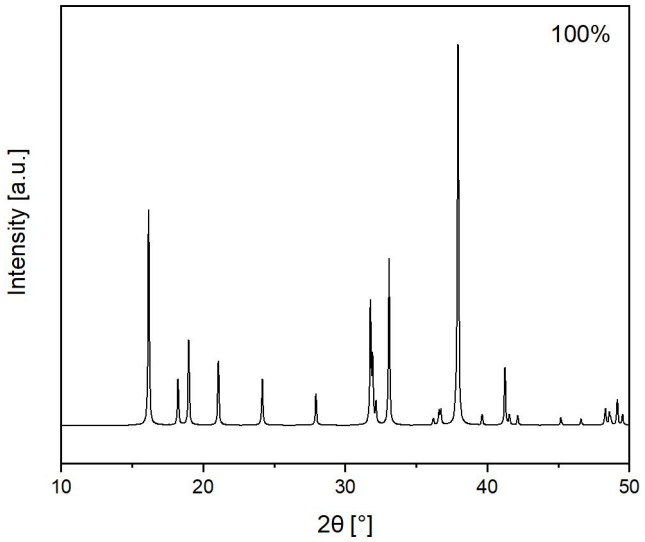

Figure S31. Simulated diffraction pattern of monoclinic Na_2ZrO_3 (*C*2/*m*) with 100% Na^+ site occupancy of the Na^+ + Zr^{4+} layer (2θ range = 10 to 50°, λ = 1.54056 Å).

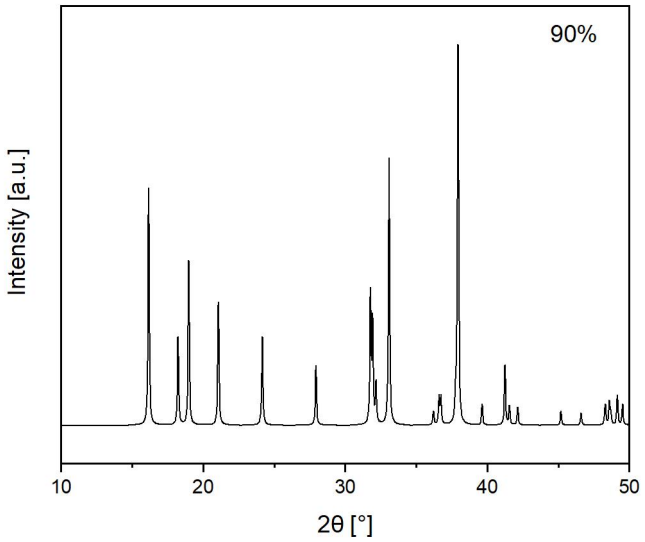

Figure S32. Simulated diffraction pattern of monoclinic Na_2ZrO_3 (*C*2/*m*) with 90% Na^+ site occupancy of the Na^+ + Zr^{4+} layer (2θ range = 10 to 50°, λ = 1.54056 Å).

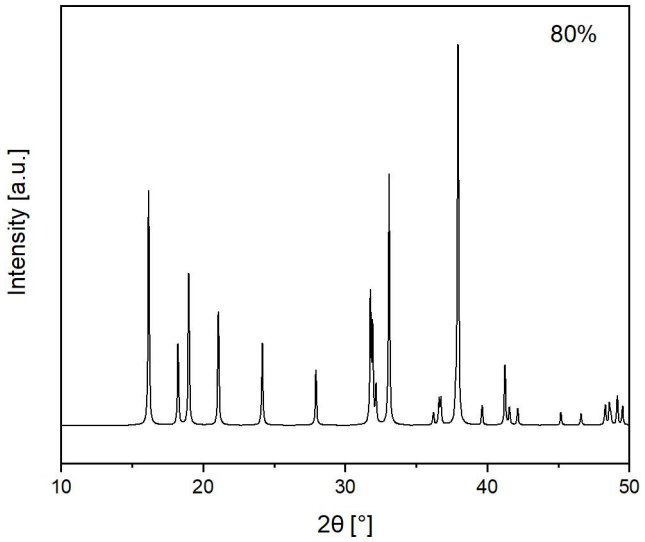

Figure S33. Simulated diffraction pattern of monoclinic Na_2ZrO_3 (*C*2/*m*) with 80% Na^+ site occupancy of the Na^+ + Zr^{4+} layer (2θ range = 10 to 50°, λ = 1.54056 Å).

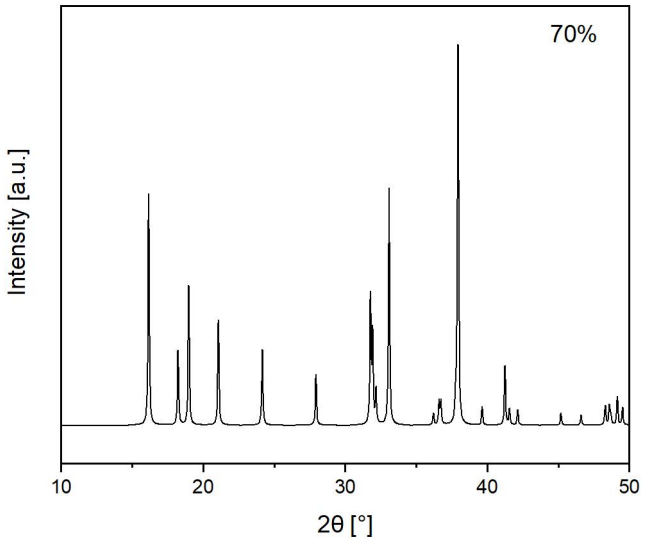

Figure S34. Simulated diffraction pattern of monoclinic Na_2ZrO_3 (C2/m) with 70% Na^+ site occupancy of the Na^+ + Zr^{4+} layer (2θ range = 10 to 50°, λ = 1.54056 Å).

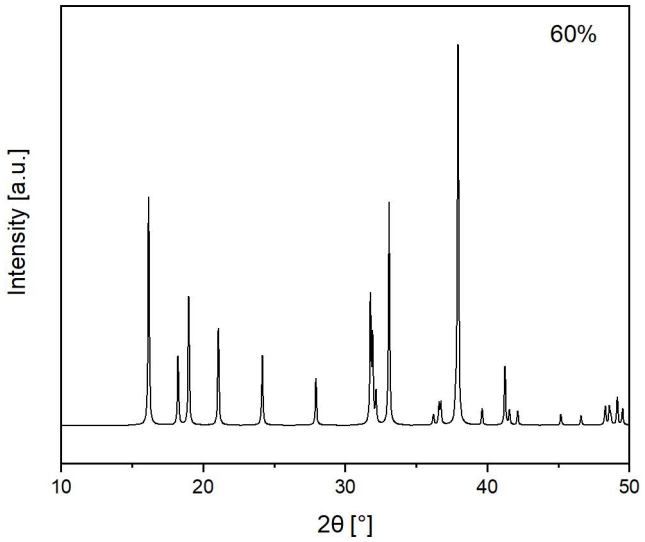

Figure S35. Simulated diffraction pattern of monoclinic Na_2ZrO_3 (*C*2/*m*) with 60% Na^+ site occupancy of the Na^+ + Zr^{4+} layer (2θ range = 10 to 50°, λ = 1.54056 Å).

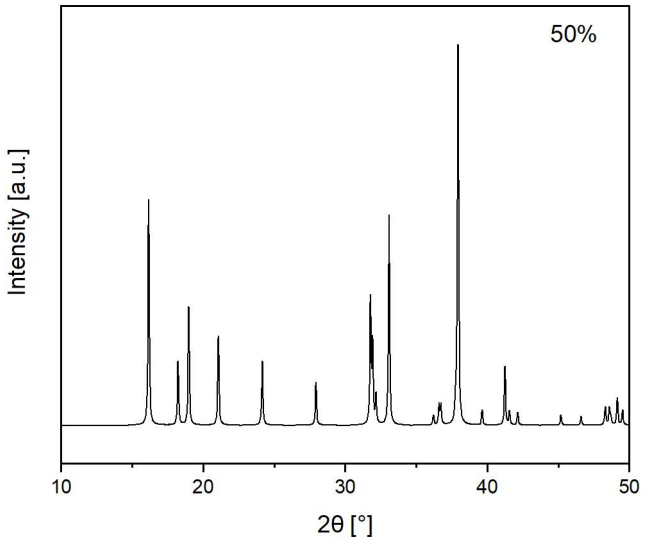

Figure S36. Simulated diffraction pattern of monoclinic Na_2ZrO_3 (*C*2/*m*) with 50% Na^+ site occupancy of the Na^+ + Zr^{4+} layer (2θ range = 10 to 50°, λ = 1.54056 Å).

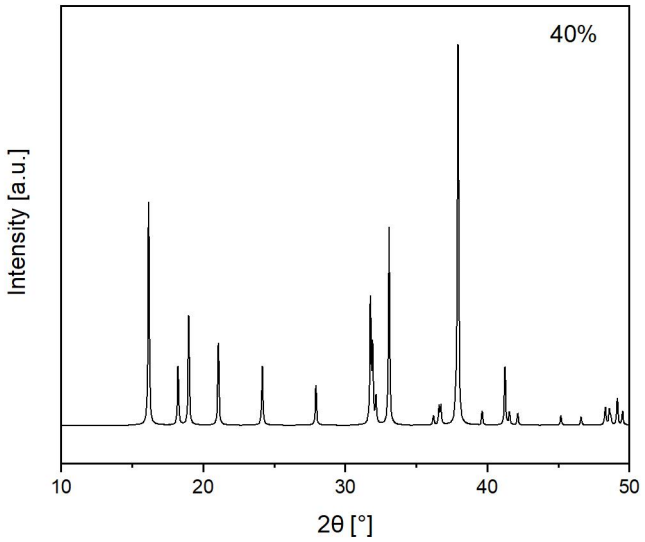

Figure S37. Simulated diffraction pattern of monoclinic Na_2ZrO_3 (*C*2/*m*) with 40% Na^+ site occupancy of the Na^+ + Zr^{4+} layer (2θ range = 10 to 50°, λ = 1.54056 Å).

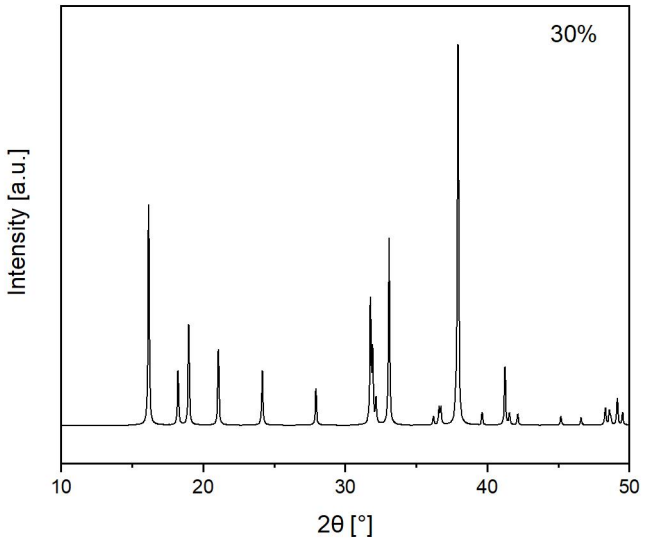

Figure S38. Simulated diffraction pattern of monoclinic Na_2ZrO_3 (*C*2/*m*) with 30% Na^+ site occupancy of the Na^+ + Zr^{4+} layer (2θ range = 10 to 50°, λ = 1.54056 Å).

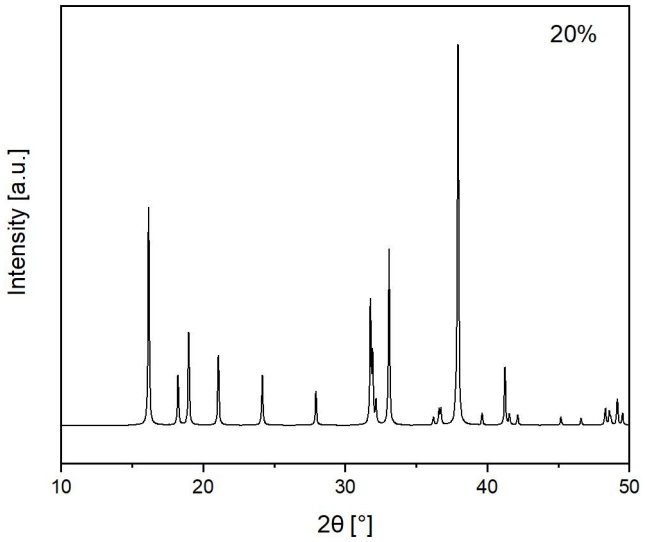

Figure S39. Simulated diffraction pattern of monoclinic Na_2ZrO_3 (*C*2/*m*) with 20% Na^+ site occupancy of the Na^+ + Zr^{4+} layer (2θ range = 10 to 50°, λ = 1.54056 Å).

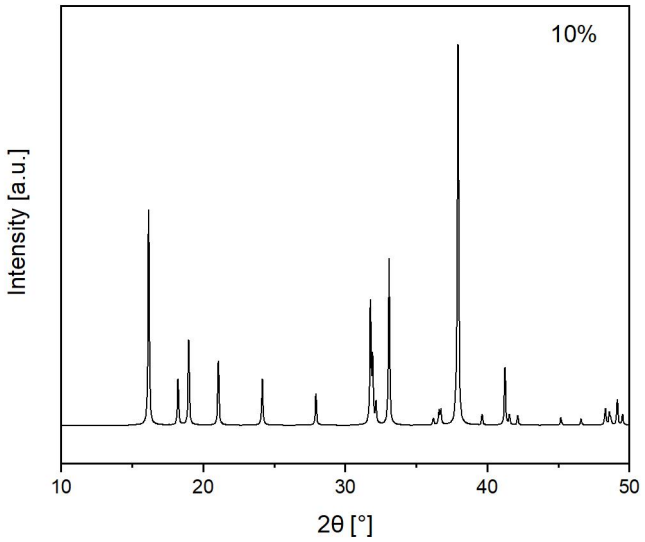

Figure S40. Simulated diffraction pattern of monoclinic Na_2ZrO_3 (*C*2/*m*) with 10% Na^+ site occupancy of the Na^+ + Zr^{4+} layer (2θ range = 10 to 50°, λ = 1.54056 Å).

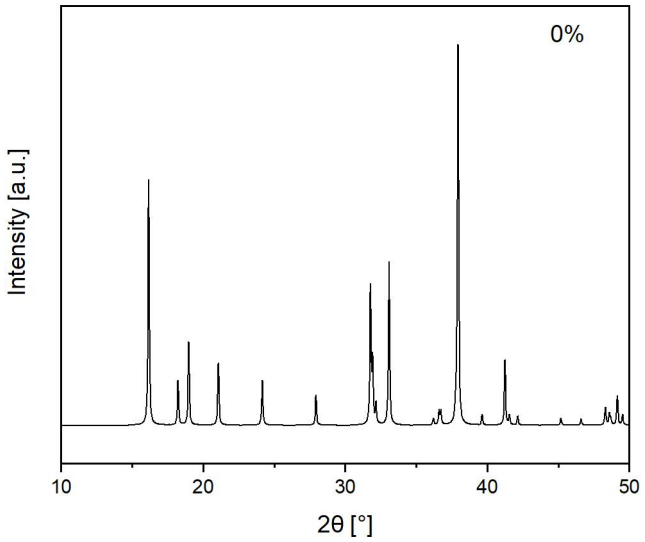

Figure S41. Simulated diffraction pattern of monoclinic Na_2ZrO_3 (*C*2/*m*) with 0% Na^+ site occupancy of the Na^+ + Zr^{4+} layer (2θ range = 10 to 50°, λ = 1.54056 Å).

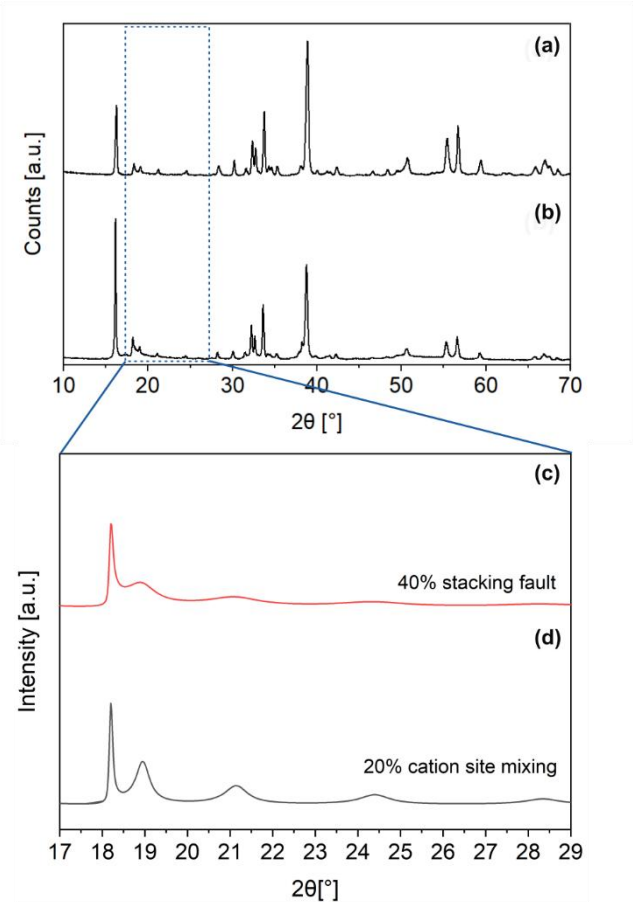

Figure S42. Estimated disorder degree in the observed diffraction patterns (from Figure 1) of the synthesized NZO-M and NZO-H using the simulated diffraction patterns of stacking fault and cation site mixing (2θ range = 17 to 29°, λ = 1.54056 Å). Both (a) NZO-M and (b) NZO-H showed the combination of (c) 40% stacking fault and (d) 20% cation site mixing.

1.4 Electronic structure calculations

Electronic structure calculations based on density functional theory (DFT) in an implementation with plane waves and pseudopotential (PWPP) have been undertaken to find support for the claims made based on experimental observations. The exchange-correlation energy was described using the functional proposed by Perdew-Burke-Ernzerhof (PBE).[43] All calculations were performed using the the Vienna Ab Initio Simulation Package (VASP) [4-7] with projector augmented wave (PAW) pseudopotentials.[8] Zirconium was described by 12 valence electrons ($4s^2 4p^6 5s^2 4d^2$), Na bu 1 valence electron ($2s^1 2p^0$) and oxygen by 6 valence electrons ($2s^2 2p^4$). The energy cut-off for the plane-wave basis set was set to 600 eV and all presented structures were optimized until the forces on each atom were below 0.02 eV/Å.

Both cell and ionic positions were optimized simultaneously until the forces on each atom were below 0.01 eV/atom and until all components of the stress tensor was smaller than 1 k bar. In the simulations, the Brillouin zone was sampled with a smallest k-point spacing of 0.28 $Å^{-1}$. Altering the k-point mesh did not significantly altered the results (within $1e^{-3}$ eV/super cell).

Table S3. The calculated DFT structural data of the optimized different space group models of *C*2/*c*, *C*2/*m*, *P*3$_1$12, and *P*3$_2$12 with total energy/formula unit (E_{DFT}).

Space group	Optimized structural data	Number of Na_2ZrO_2 formula units (f.u.)	E_{DFT} [eV/f.u.]
*C*2/*c*	a = 5.6398 Å b = 9.7852 Å c = 33.3253 Å α = 90.0000° β = 100.0630° γ = 90.0000°	24	−41.676
*C*2/*m*	a = 5.6416 Å b = 9.7836 Å c = 32.8156 Å α = 89.6290° β = 90.2263° γ = 90.1070°	24	−41.675
*P*3$_1$12	a = 5.6449 Å b = 9.7772 Å c = 32.8131 Å α = 90.0000° β = 90.0056° γ = 90.0000°	24	−41.676
*P*3$_2$12	a = 5.6454 Å b = 9.7773 Å c = 32.8064 Å α = 90.0001° β = 90.0241° γ = 90.0000°	24	−41.676

Section 2. Thermodynamic stability measurement

CO_2 uptake properties were examined using a Mettler Toledo TGA2 thermogravimetric analysis (Schwerzenbach, Switzerland) on the as-synthesized **NZO-M** and **NZO-H** samples. Over 20 carbonation/calcination cycles were performed at 750/900 °C for up to 20 min using 100% CO_2 for carbonation and N_2 for calcination with a flow rate of 100 mL/min. After cycling, PXRD patterns of both **NZO-M** and **NZO-H** were collected.

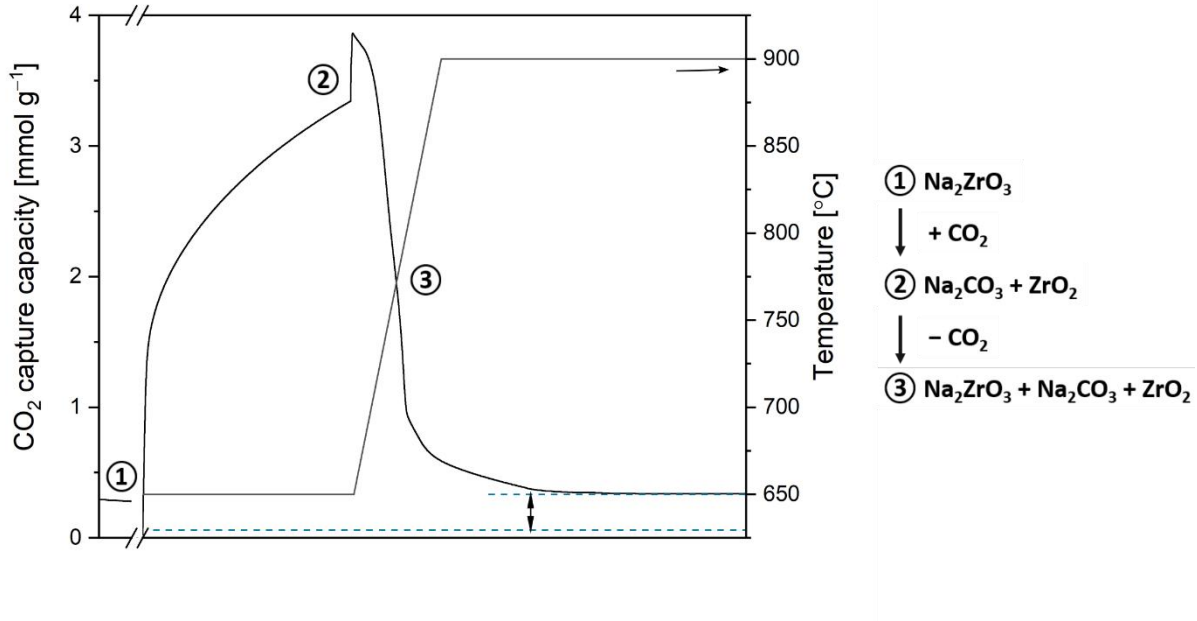

Figure S43. Typical TGA profile of one carbonation/calcination cycle at 750°C and 900°C, respectively, with Na_2ZrO_3 as the CO_2 sorbent.

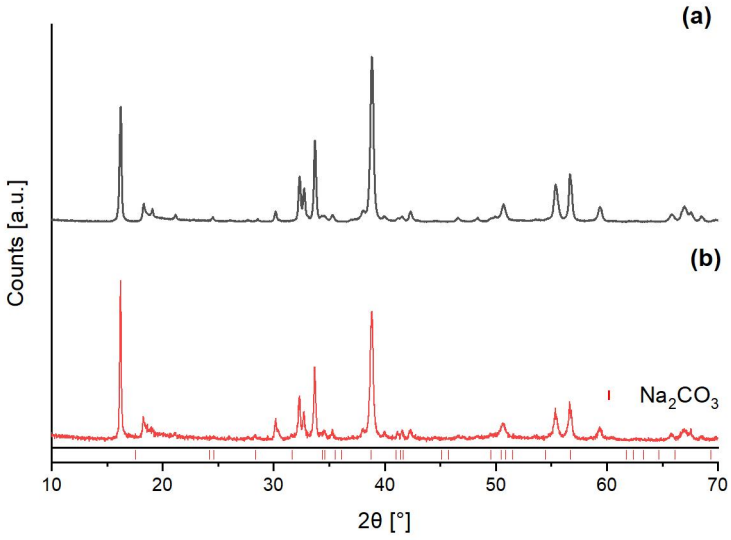

Figure S44. PXRD patterns of (a) as synthesized NZO-M (b) after one carbonation/calcination cycle (calcined NZO-H).

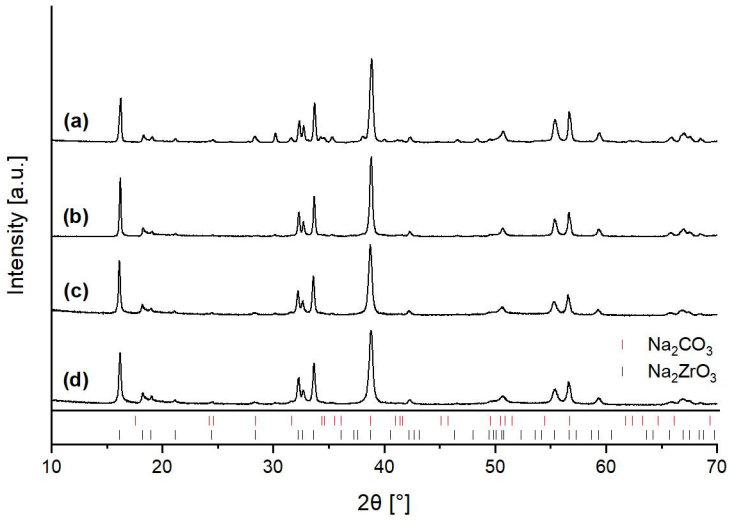

Figure S45. PXRD patterns of the as synthesized Na_2ZrO_3 with Na_2CO_3:ZrO_2= (a) 1.5 (b) 1.25 (c) 1 (d) 0.75:1, synthesized at 900 °C with 5 °C/min of heating rate and 100 ml/min of 100% nitrogen (N_2) for 2 hrs.

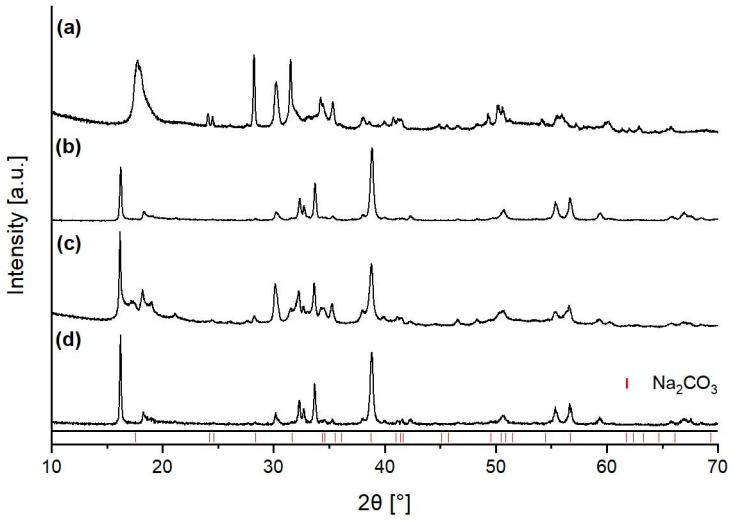

Figure S46. PXRD patterns of after one carbonation/calcination cycle of the synthesized Na_2ZrO_3 with Na_2CO_3:ZrO_2= (a) 1.5 (b) 1.25 (c) 1 (d) 0.75:1, synthesized at 900 °C with 5 °C/min of heating rate and 100 ml/min of 100% nitrogen (N_2) for 2 hrs.

Table S4. The relative intensity of major peaks of Na_2ZrO_3 depending on the simulations of stacking faults and cation mixing.

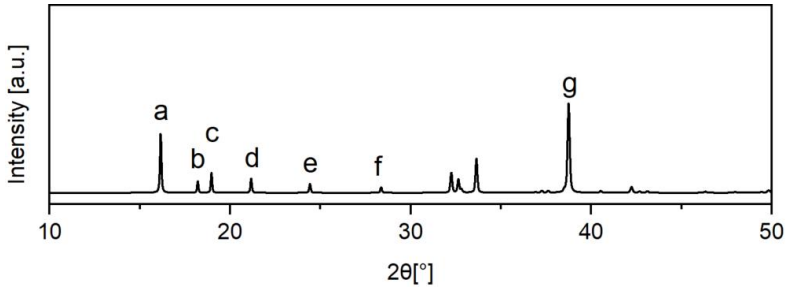

	I_a/I_{max}	I_b/I_{max}	I_c/I_{max}	I_d/I_{max}	I_e/I_{max}	I_f/I_{max}	I_g/I_{max}
0% of Stacking faults	0.66	0.13	0.22	0.16	0.10	0.06	1.00
10% of Stacking faults	0.66	0.12	0.08	0.03	0.02	0.01	1.00
20% of Stacking faults	0.66	0.10	0.04	0.02	0.01	0.01	1.00
30% of Stacking faults	0.66	0.09	0.03	0.01	0.01	N/A	1.00
40% of Stacking faults	0.66	0.08	0.03	0.01	0.01	N/A	1.00
50% of Stacking faults	0.66	0.08	0.02	0.01	N/A	N/A	1.00
60% of Stacking faults	0.66	0.07	0.02	0.01	N/A	N/A	1.00
70% of Stacking faults	0.66	0.07	N/A	N/A	N/A	N/A	1.00
80% of Stacking faults	0.66	0.07	N/A	N/A	N/A	N/A	1.00
90% of Stacking faults	0.66	0.07	N/A	N/A	N/A	N/A	1.00

100% of Stacking faults	0.66	0.07	N/A	N/A	N/A	N/A	1.00
0% of cation mixing	0.66	0.13	0.22	0.16	0.10	0.06	1.00
10% of cation mixing	0.66	0.10	0.17	0.12	0.07	0.04	1.00
20% of cation mixing	0.66	0.07	0.12	0.08	0.05	0.03	1.00
30% of cation mixing	0.66	0.04	0.07	0.05	0.03	0.02	1.00
40% of cation mixing	0.66	0.03	0.04	0.03	0.02	0.01	1.00
50% of cation mixing	0.66	0.01	0.02	0.01	0.01	-	1.00

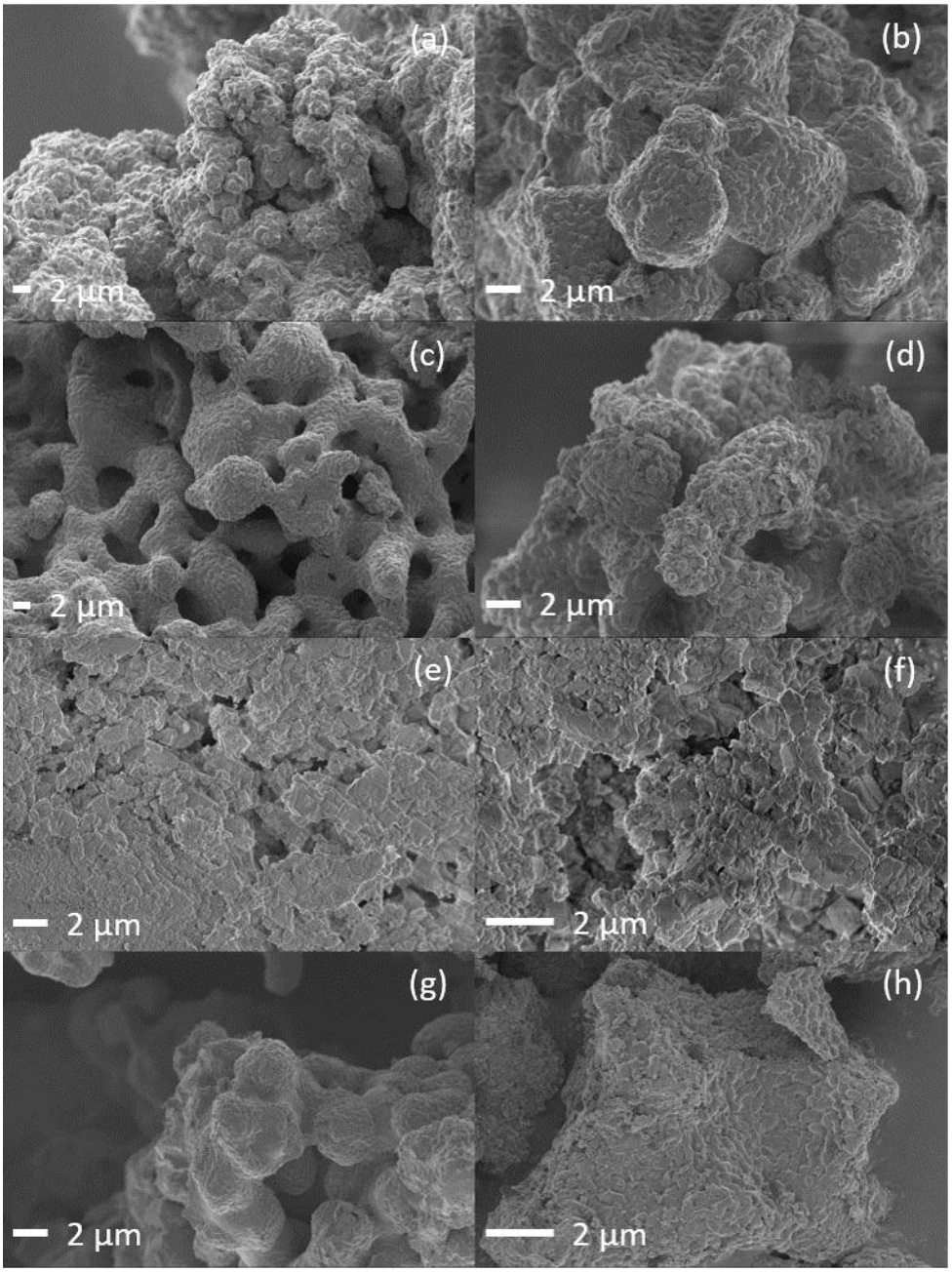

Figure S47. Scanning electron micrograph of **NZO-M** before performing the cyclic stability test (a) at 5.00 K X (b) at 10.00 K X, **NZO-M** after performing the cyclic stability test (c) at 5.00 K X (d) at

10.00 K, **NZO-H** before performing the cyclic stability test (e) at 10.00 K X (f) at 20.00 K X, **NZO-H** after performing the cyclic stability test (g) at 5.00 K X (h) 10.00 K X.

Reference

1. Bareño, C. H. Lei, J. G. Wen, S. -H. Kang, I. Petrov, and D. P. Abraham, J. *Adv. Mater.*, 2010, **22**, 1122-1127.
2. K. Momma and F. J. Izumi, *J. Appl. Crystallogr.*, 2008, **41**, 653-658.
3. J. P. Perdew, K. Burke, and M. Ernzerhof, *Phys. Rev. Lett.* 1996, **77**, 3865-3868.
4. G. Kresse and J. Furthmüller, *Phys. Rev. B*, 1996, **54**, 11169-11186.
5. G. Kresse and J. Furthmüller, *Comput. Mater. Sci.*, 1996, **6**, 15-50.
6. G. Kresse and J. Hafner, *Phys. Rev. B*, 1993, **47**, 558–561.
7. G. Kresse and J. Hafner, *Phys. Rev. B,* 1994, **49**, 14251-14269.
8. P. E. Blöchl, C. J. Först, and J. Schimpl *Bull. Mater. Sci.*, 2003, **26**, 33-41.